Rare-earth–boron bonding and 4f state trends in $\mathcal{R}B_4$ tetraborides

Z. P. Yin and W. E. Pickett
Department of Physics, University of California Davis, Davis, CA 95616
(Received 19 July 2007; published 31 January 2008)

The B–B bonding, boron–rare earth coupling, and the changes in 4*f* states across the lanthanide series in RB_4 (R=rare earth) compounds are studied using the correlated band theory LDA+U method. A set of boron bonding bands that are well separated from the antibonding bands can be identified. Separately, the "dimer B" $2p_z$ orbital is nonbonding (viz., graphite and MgB_2), but mixes strongly with the metal 4*d* or 5*d* states that form the conduction states. The bonding bands are not entirely filled even for the trivalent compounds (thus the cation *d* bands have some filling), which accounts for the lack of stability of this structure when the cations are divalent (with more bonding states unfilled). The trends in the mean 4*f* level for both majority and minority, and occupied and unoccupied, states are presented and interpreted.

DOI: 10.1103/PhysRevB.77.035135 PACS number(s): 71.28.+d, 71.20.−b, 71.20.Eh

I. BACKGROUND AND MOTIVATION

The tendency of the metalloid boron to form clusters has led to widespread study of the properties of condensed boron. Of the many classes of compounds that B forms, B-rich metal borides include classes with very important, and intensely studied, properties. One example is MgB_2, which is the premier phonon-coupled superconductor[1] (at 40 K). Although this structural class includes several transition metal borides and other simple metal borides (such as LaB_2), MgB_2 is unique in this single-member class of quasi-two-dimensional *s-p* metal with very high superconducting transition temperature due to strong covalent B–B bonds that are driven metallic[2] by the crystal structure and chemistry.

Another class that has received great attention is the hexaborides MB_6 formed from vertex-linked B_6 octahedra that enclose the metal ion in the cubic interstitial site. This class includes the divalent metals (M=Ca,Sr,Ba) that are small gap semiconductors.[3–12] The stability of this structure was understood decades ago, when cluster studies established[3,4] that the bonding states of linked B_6 clusters are filled by 20 electrons, which requires two per B_6 unit in addition to the B valence electrons. There are many trivalent hexaborides as well, including lanthanide members which have very peculiar properties: unusual magnetic ordering, heavy fermion formation, and superconductivity.[6,7,11,13–16] Two monovalent members, NaB_6 (Ref. 17) and KB_6 (Ref. 18), have been reported.

Yet another class that has been known for decades is the metal (mostly rare earths) tetraboride RB_4 family, which is richer both structurally and electronically and for which considerable data are available (see, for several RB_4, Refs. 19–22; YB_4, Refs. 23–27; LaB_4, Ref. 28; CeB_4, Refs. 29–31; NdB_4, Ref. 32; GdB_4, Refs. 33–38; TbB_4, Refs. 39–44; DyB_4, Refs. 45–50; and ErB_4, Refs. 44, 51, and 52). Yttrium and all the lanthanides except Eu and Pm form isostructural metallic tetraborides RB_4 with space group $P4/mbm$ (No. 127), described below and pictured in Fig. 1. Presumably Eu is not stable in the tetraboride structure because of its preference for the divalent configuration in such compounds. The Sr and Ba tetraborides also are not reported. A "calcium tetraboride" with formula $Ca(B_{1-x}C_x)_4$, $x \approx 0.05$ was reported[53] recently.

These rare-earth tetraborides exhibit an unusual assortment of magnetic properties. While CeB_4 and YbB_4 (f^1 and f^{13}, respectively) do not order and PrB_4 orders ferromagnetically at T_C=25 K,[36] all of the others (R=Nd,Sm,Gd,Tb,Dy,Ho,Er,Tm) order antiferromagnetically, with Néel temperature T_N (see Table I) spanning the range 7–44 K. A noteworthy peculiarity is that T_N does not obey de Gennes scaling law, which says that the magnetic transition temperature is proportional to $(g_J-1)^2J(J+1)$ across an isostructural series where the rare-earth atom is the only magnetic component.[43,54] (Here J is Hund's rule total angular momentum index, and g_J is the corresponding Landé g factor.) In the rare-earth nickel borocarbide series, for example, de Gennes scaling is obeyed faithfully.[55] This lack of

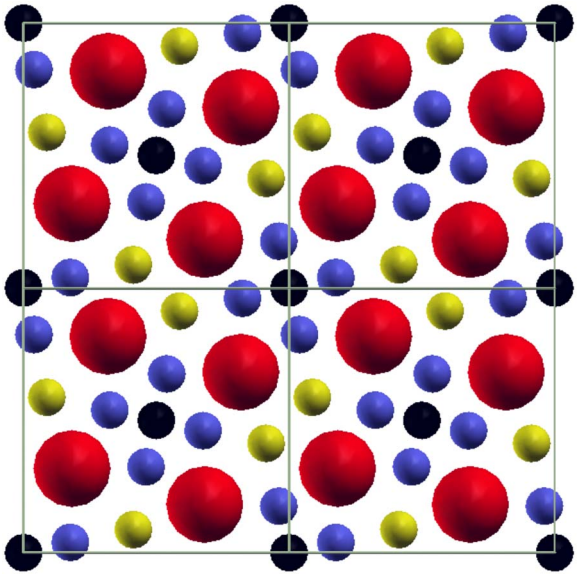

FIG. 1. (Color online) Structure of RB_4 viewed from along the c direction. The large metal ion spheres (red) lie in z=0 plane. Apical B1 atoms (small black) lie in $z \simeq 0.2$ and $z \simeq 0.8$ planes. Lightly shaded (yellow) dimer B2 and equatorial B3 (dark, blue) atoms lie in z=0.5 plane. The sublattice of R ions is such that each one is a member of two differently oriented R_4 squares, and of three R_3 triangles.

TABLE I. Data on magnetic ordering in the RB_4 compounds. (Refs. 19, 21, 36, and 50). The columns provide the experimental ordering temperature(s) T_{mag}, the ordering temperature T_{th} predicted by de Gennes law (relative to the forced agreement for the GdB_4 compound), the orientation of the moments, and the measured ordered moment compared to theoretical Hund's rule moment (μ_B).

	T_{mag} (K)	T_{th} (K)	Direction	μ(exp)	μ(th)
PrB_4	24	2.1	$\|c$	3.20	3.58
SmB_4	26	12			0.84
GdB_4	42	42	$\perp c$	7.81	7.94
TbB_4	44, 24	28	$\perp c$	9.64	9.72
DyB_4	20.3, 12.7	19	$\|c$	10.44	10.63
HoB_4	7.1, 5.7 (1st)	12	$\|c$	10.4	10.6
ErB_4	15.4	7	$\|c$	9.29	9.60
TmB_4	11.7, 9.7(1st)	3	$\perp c$	7.35	7.56

scaling indicates that magnetic coupling varies across the series, rather than following a simple Ruderman-Kittel-Kasuya-Yosida (RKKY)-like[56] behavior with a fixed Fermi surface.

Both the ferromagnetic member PrB_4 and antiferromagnetic ones RB_4 show strong magnetic anisotropy. For ferromagnetic PrB_4 the c axis is the easy axis. The situation is more complicated for the antiferromagnetic compounds, which display varying orientations of their moments below T_N, and some have multiple phase transitions. GdB_4 and ErB_4 have only one second order phase transition, while both TbB_4 and DyB_4 have consecutive second order phase transitions at distinct temperatures. A yet different behavior is shown by HoB_4 and TmB_4, which have a second order phase transition followed by a first order phase transition at lower temperature. The magnetic ordering temperatures, primary spin orientations, and experimental and theoretical effective (Curie-Weiss) magnetic moments have been collected in Table I.

The variety of behaviors displayed by these tetraborides suggests a sensitivity to details of the underlying electronic structure. Unlike the intense scrutiny that the tetraborides have attracted, there has been no thorough study of the tetraboride electronic structure, which contains a new structural element (the "boron dimer") and an apical boron that is inequivalent to the equatorial boron in the octahedron. We provide here a detailed analysis, beginning with the reference compound YB_4 which allows an analysis of the itinerant bands without the complications of $4f$ orbitals. Then we proceed to provide an initial look into the trends to be expected in the $4f$ shells of the rare-earth ions.

II. CRYSTAL STRUCTURE

The full RB_4 structure was first reported by Zalkin and Templeton[31] for the Ce, Th, and U members. These tetraborides crystallize at room temperature in the tetragonal space group $P4/mbm$, D_{4h}^5 with four formula units occupying the positions listed in Table II. The lattice constants for the reported rare-earth tetraborides are presented in Table III.

The B1 and B3 atoms form B_6 octahedra (apical and equatorial vertices, respectively) that are connected by B2 dimers in the $z=1/2$ plane. The B_6 octahedra, which are arrayed in centered fashion in the x-y plane within the cell, are flattened somewhat, with distances from the center being 1.20 Å along the c axis and 1.29 Å in the x-y plane (taking GdB_4 as an example). Each B2 atom is bonded to two B1 atoms in separate octahedra and to one other B2 atom. A suggestive form for the chemical formula then is $[R_2B_2B_6]_2$. The rare-earth atoms lie in the large interstitial holes in the $z=0$ plane, and form a two-dimensional array that can be regarded as fused squares and rhombuses.[35]

The R site symmetry is mm. The symmetry of an R site is important for the magnetic properties of the compounds, as it dictates the crystal field splitting of the ion with total angular momentum $\vec{J}=\vec{L}+\vec{S}$ and thereby the resulting magnetic state at low temperature. The R ion is coordinated by seven B atoms in planes both above and below, three of them being dimer B2 atoms (two 2.88 Å distant and one at a distance of 3.08 Å) and four of them equatorial B3 atoms (two each at distances of 2.76 and 2.84 Å). Within the unit cell the four R sites form a square of side $d=0.518a=3.70$ Å, oriented at about 15° with respect to the square sublattice of B_6 octahedra. The (low) site symmetries of the apical B1, dimer B2, and equatorial B3 atoms are 4, mm, and m, respectively.

The reported lattice constants for the lanthanides are plotted in Fig. 2. It is evident that most fall on smooth lines reflecting the lanthanide contraction in this system. The behavior is representative of trivalent behavior, from La to Lu. The big exception is Ce, which has smaller volume suggesting that, rather than being simple trivalent, the $4f$ electron is participating in bonding. Pm with all unstable isotopes has not been reported. EuB_4 also has not been reported; Eu typically prefers the divalent state (due to the gain in energy of the half-filled $4f$ shell) so it is not surprising that it is differ-

TABLE II. Site designations, symmetries, and atomic positions of the atoms in the RB_4 crystal.

R	$4g$	mm	$(x, \frac{1}{2}+x, 0)$
B1	$4e$	4	$(0, 0, z)$
B2	$4h$	mm	$(x, \frac{1}{2}+x, \frac{1}{2})$
B3	$8j$	m	$(x, y, \frac{1}{2})$

TABLE III. Tabulation of the lattice constants and internal structural parameters used in our calculations. The regularity of the internal coordinates through this system is clear, and makes the irregularity in z_{B1} for Dy of some concern. See the text for discussion.

R	a (Å)	c (Å)	x_R	z_{B1}	x_{B2}	x_{B3}	y_{B3}	Ref.
Y	7.111	4.017	0.318	0.203	0.087	0.176	0.039	23
La	7.324	4.181	0.317	0.209	0.088	0.174	0.039	22 and 28
Ce	7.208	4.091	0.318	0.203	0.087	0.176	0.039	22 and 30
Pr	7.235	4.116	0.318	0.203	0.087	0.176	0.039	21
Nd	7.220	4.102	0.318	0.203	0.087	0.176	0.039	22 and 32
Pm	7.193	4.082	0.318	0.203	0.087	0.176	0.039	
Sm	7.179	4.067	0.318	0.203	0.087	0.176	0.039	21
Eu	7.162	4.057	0.318	0.203	0.087	0.176	0.039	
Gd	7.146	4.048	0.317	0.203	0.087	0.176	0.038	35
Tb	7.120	4.042	0.317	0.202	0.087	0.176	0.039	41 and 43
Dy	7.097	4.016	0.319	0.196	0.086	0.175	0.039	21 and 51
Ho	7.085	4.004	0.318	0.203	0.087	0.176	0.039	21
Er	7.071	4.000	0.318	0.203	0.086	0.177	0.038	43 and 51
Tm	7.057	3.987	0.318	0.203	0.087	0.176	0.039	22
Yb	7.064	3.989	0.318	0.203	0.087	0.176	0.039	22
Lu	7.036	3.974	0.318	0.203	0.087	0.176	0.039	22

ent. However, some divalent tetraborides do form in this structure (e.g., CaB_4, see Sec. IV) so it cannot be concluded that EuB_4 is unstable simply on the basis of divalency. Finally, the small deviation of Yb from the smooth curves suggests that it may be mixed or intermediate valent (although close to trivalent).

III. CALCULATIONAL METHODS

The full potential local orbital (FPLO) code[57] (version 5.18) was used in our calculations. Both LDA (PW92 of Perdew and Wang[58]) and LDA+U (using the atomic limit functional) are used. We used a k mesh of 12^3 in the full Brillouin zone. For the density of states (DOS) plot and Fermi surface plot, we used a k mesh of 24^3 for more precision. The basis set was $1s2s2p3s3p3d4s4p::(4d4f5s5p)/6s6p5d+$ for all metal elements {except Y$[1s2s2p3s3p3d::(4s4p)/5s5p4d+]$ and Ca$[1s2s2p::(3s3p)/4s4p3d+]$}. For boron atoms we used the basis $::1s/(2s2p3d)+$.

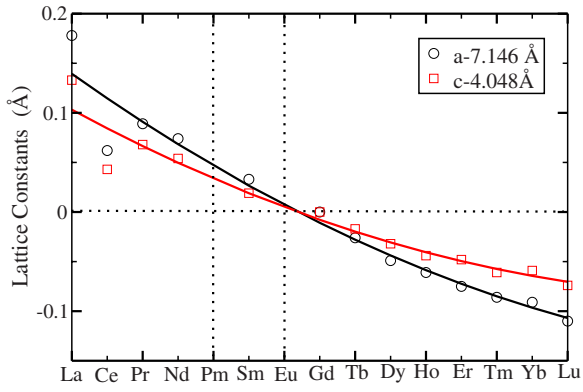

FIG. 2. (Color online) Plot of experimental lattice constants of RB_4 vs position in the Periodic Table (atomic number), showing a lanthanide contraction of about 5% for a and 3% for c. The smooth lines show a quadratic fit to the data.

In the LDA+U calculations we used values typical for $4f$ atoms $U=8$ eV and $J=1$ eV (corresponding to Slater integrals $F_1=8.00$, $F_2=11.83$, $F_4=8.14$, and $F_6=5.86$) throughout all calculations. The high symmetry points in the tetragonal zone are $\Gamma=(0,0,0)$, $X=(\frac{\pi}{a},0,0)$, $M=(\frac{\pi}{a},\frac{\pi}{a},0)$, $Z=(0,0,\frac{\pi}{c})$, $R=(\frac{\pi}{a},0,\frac{\pi}{c})$, and $A=(\frac{\pi}{a},\frac{\pi}{a},\frac{\pi}{c})$.

The experimental structures (Table II) were used for our calculations. The reported value of $z_{B1}=0.196$ for DyB_4 differs from the others, which all have $z_{B1}=0.202-0.203$. Using a dense sampling k mesh of $24\times24\times24$ points in the zone, we compared energies for GdB_4 and DyB_4. The results were, for the two values of z_{B1},

$$GdB_4\ E(0.203)-E(0.196)=-263\ \text{meV},$$

$$DyB_4\ E(0.203)-E(0.196)=+17\ \text{meV}.$$

Hence the Dy compound does display some energetic difference from the Gd compound (and presumably from the others). The difference in the B1 position is no more than 0.03 Å, and this amount is not enough to affect appreciably the trends we discuss in this paper. Whether this softness in the B1 position is related to the structural transition observed in DyB_4 (Ref. 59) is a question for further studies.

The crystal structure in Fig. 1 was rendered graphically with the XCRYSDEN software.[60]

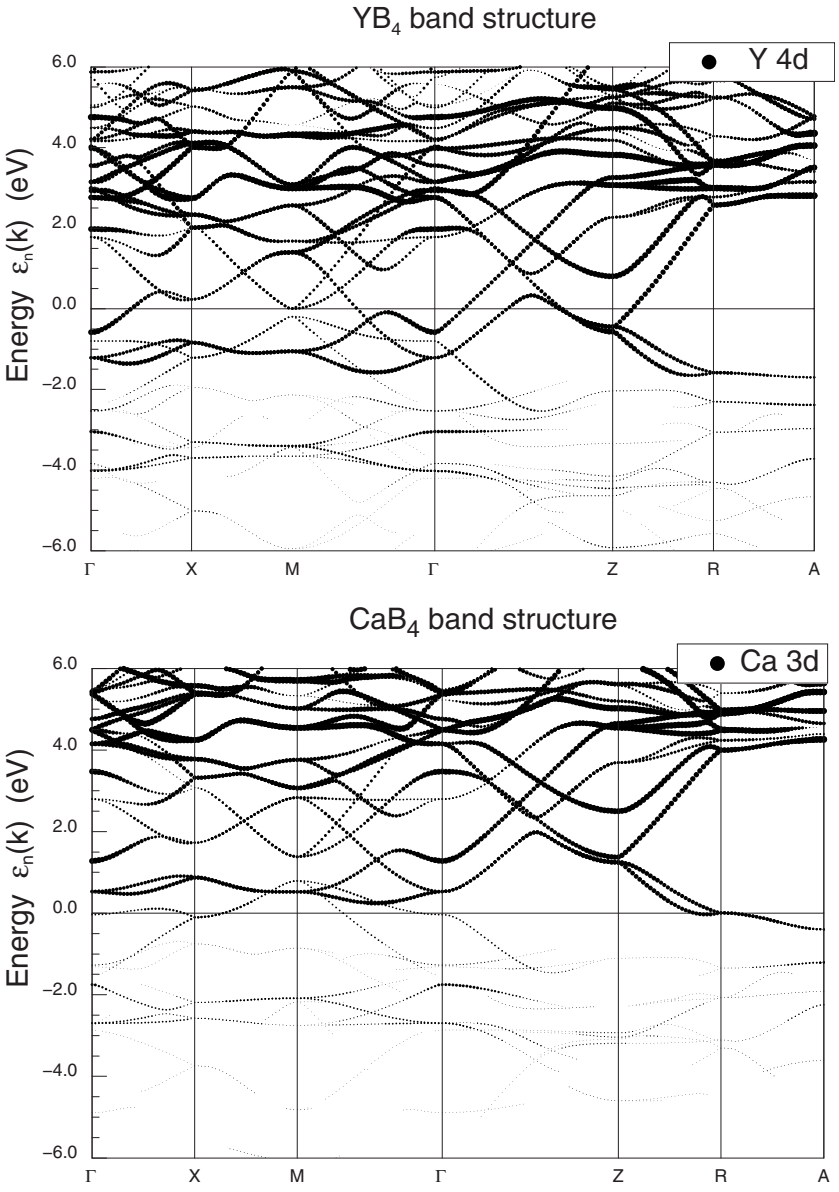

FIG. 3. Band structure of YB_4 (top panel) and CaB_4 (lower panel) within 6 eV of the Fermi level along high symmetry directions, showing the gap that opens up around E_F (taken as the zero of energy) throughout much of the top and bottom portions of the tetragonal Brillouin zone. Notice the lack of dispersion along the upper and lower zone edges *R*-*A*-*R* ($k_z=\pi/c$, and either k_x or k_y is π/a). Note also that, due to the nonsymmorphic space group, bands stick together in pairs along *X*-*M* (the zone "equator") and along *R*-*A* (top and bottom zone edges).

IV. GENERAL ELECTRONIC STRUCTURE

The valence-conduction band structure of YB_4 (where there are no 4*f* bands) is shown in Fig. 3. For LaB_4, which differs in volume and conduction *d* level position, the bands are very similar, with only slightly differing Fermi level crossings along the *M*-Γ direction. The occupied valence bandwidth is 11 eV (not all bands are shown in this figure). One striking feature of the bands is the broad gap of more than 3 eV along the top (and bottom) edges *R*-*A*-*R* of the Brillouin zone. Bands along these lines stick together in pairs due to the nonsymmorphic space group, and nearly all bands disperse very weakly with k_x (or k_y) along these edges. This gap closes along the $k_z=\pi/c$ plane of the zone only for small in-plane components of the wave vectors. It is such gaps enclosing E_F that often account for the stability of a crystal structure, and the stability of boride structures, including this one, has been a topic of interest for decades.[3,4,61,62]

The band structure of a divalent cation member (CaB_4) is also included in Fig. 3 for comparison. The largest difference is the band filling, as expected, although some band positions differ in important ways near the Fermi level. Still the 3*d* bands of Ca are not quite empty, as a band with substantial 3*d* character lies at E_F at *R* and is below E_F all along the *R*-*A* line. CaB_4 can be fairly characterized, though, as having nearly filled bonding B 2*p* bands and nearly empty Ca 3*d* bands.

A. Bonding and antibonding bands

As mentioned in the Introduction, the stability of the hexaborides is understood in terms of ten bonding molecular orbitals of the B_6 octahedron. This octahedron occurs also in these tetraborides, along with one additional B_2 dimer that is bonded only in the layer (sp^2). Lipscomb[3,4] started from this point, and argued that each of the B2 atoms in a dimer forms single bonds with two B3 atoms but a double bond with its dimer neighbor, so each B2 atom needs four electrons. The total of 20+8 electrons for each set of 6+2 boron atoms

leaves a deficit of four electrons, or a deficit of 8 electrons in the cell. This amount of charge can be supplied by four divalent cations, with CaB_4 as an example. Most tetraborides contain trivalent cations, however, so this is an issue worth analyzing.

An empirical extended Hückel band structure study[53] for CaB_4 indeed gave a gap, albeit a very narrow one. The Hückel method can be very instructive but is not as accurate as self-consistent density functional methods. Our FPLO calculation on CaB_4, shown in Fig. 3, gives a metallic band structure. However, the "valence" (occupied) and "conduction" (unoccupied) bands (Hückel, and also FPLO) are readily identified, and it is clear that there are disjoint sets of bands with different characters. There are the boron bonding bands (at E_F and below) that can be clearly distinguished from conduction bands at and above E_F. These conduction bands are primarily metal d bands (with an interspersed nonbonding B2 p_z band, see below). If they were ~0.5 eV higher it would result in an insulating band structure in CaB_4. The boron antibonding bands lie higher, above 5 eV at least and mix strongly with the metal d bands.

The separation into bonding and antibonding B $2p$ bands agrees (almost) with the ideas of Lipscomb,[3,4] and confirms his counting arguments. However, the existence of numerous $R^{3+}B_4$ compounds and only one divalent member shows that the extra electron is not a destabilizing influence, while it increases the conduction electron density (hence, the conductivity and magnetic coupling).

In covalently bonded materials it is common to be able to identify the distinction between the bonding bands and the antibonding bands. In covalent semiconductors, for example, they lie, respectively, below and above the band gap, an absolutely clean separation. In the RB_4 system the d bands lie within the corresponding bonding-antibonding gap and complicate the picture. Analysis of the orbital-projected bands clarifies this aspect. The B1 and B3 atoms, being engaged in three-dimensional bonding (within an octahedron *and* to another unit [octahedron or dimer]), have a clear bonding-antibonding splitting of a few eV (beginning just below E_F). Likewise, the dimer B2 p_x,p_y states display a similar splitting.

The B2 p_z orbital is quite different. As is the case in MgB_2 (whose planar structure is similar to the local arrangement of a B2 atom), p_z bands extend continuously through the gap in the B bonding and/or antibonding bands, and mix fairly strongly with the rare-earth d states in that region. There is considerable B2 p_z character in the bands near (both below and above) E_F at the zone edge M point, as well as the Y $4d$ character that is evident in Fig. 3. So while there is some B1 and B3 characters in the rare-earth metal d bands that lie within the boron bonding-antibonding gap, the amount of B2 p_z character is the primary type of B participation in these bands that provide conduction and magnetic coupling.

B. Pseudogap in the density of states

From the projected DOS of the three types of B atoms of YB_4 (see Fig. 4), one can detect only relatively small differences in the distribution of B1, B2, and B3 characters arising from their differing environments. First, note that in the DOS of B1 and B3 there is a peak around −15 eV, while there is no such peak for B2. This peak arises from the overlap of $2s$ and $2p_\sigma$ states of each of the boron atoms forming the B_6 octahedra (B1 and B3); the $2s$ character is about three times as large as the $2p_\sigma$ character, and the remaining $2s$ character is mixed into the lower $2p$ bands. This state is a well localized B_6 cluster orbital, and there are two such orbitals (octahedral clusters) per cell. The bridging B2 atoms do not participate in any such bound state.

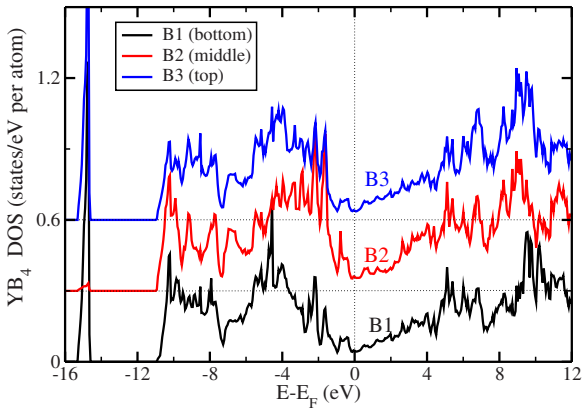

FIG. 4. (Color online) Projected density of states per atom of each of the B atoms for YB_4. The curves are shifted to enable easier identification of the differences. The B $2p$ bonding-antibonding gap can be identified as roughly from −1 eV to 4−5 eV.

Another difference in characters of the B sites is that, in the region below but within 2 eV of the Fermi level, the DOS of the dimer B2 atom is significantly larger than that of B1 and B3 atoms, as can be seen in Fig. 5. Together with plots showing the band character (not shown), this difference reflects the fact that all of the $2p$ orbitals of B1 and B3 (octahedron) atoms are incorporated into bonding (filled) and antibonding (empty) bands. The distinct characteristic of the

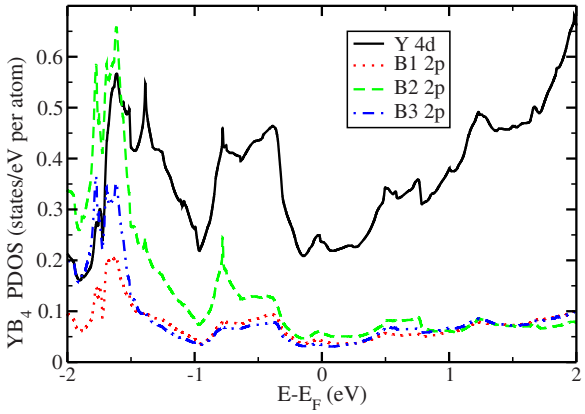

FIG. 5. (Color online) Enlargement of the partial densities of states of Y $4d$ and B $2p$ states (per atom) near the Fermi level. The states at the Fermi level, and even for almost 2 eV below, have strong $4d$ character. The apical B2 character is considerably larger than that of B1 or B3 in the two peaks below E_F, but is only marginally larger exactly at E_F.

B2 p_z state was discussed in the previous subsection. All B $2p$ states do hybridize to some degree with the metal d bands, however, and all B atoms have some contribution at the Fermi level.

The full Y $4d$ DOS (not shown) establishes that these bands are centered about 4 eV above E_F, with a "bandwidth" (full width at half maximum) of 6–7 eV (a "full bandwidth" would be somewhat larger). The largest Y character near E_F along symmetry lines is $4d(x^2-y^2)$, primarily in the bands dispersing up from −0.5 eV at Z toward Γ. The flatbands around −1 eV along Γ-X-M-Γ are strongly $4d(z^2)$ character, indicative of a nonbonding, almost localized state in the x-y plane. Note that these bands disperse strongly upward along $(0,0,k_z)$ and lie 3–4 eV above E_F in the $k_z=\pi/c$ plane. Thus the $4d(z^2)$ orbitals form two nearly separate one-dimensional bands along k_z, and give rise to flat parts of some Fermi surfaces (see following subsection). These bands can be modeled by a tight-binding band $-t_{dd\sigma}\cos k_z c$ with hopping amplitude $t_{dd\sigma}\approx 1$ eV. Most of the $4d(xz)$, $4d(yz)$ character and $4d(xy)$ character lie above E_F, and are centered 3–4 eV above E_F. The B2 $2p_z$ state mixes primarily with Y $4d_{xz}$, $4d_{yz}$ near the M point (near E_F and above). The B2 $2p_z$ orbitals are shifted up somewhat with respect to the $2p_x$ and $2p_y$ states by the ligand field effects (there is a bonding interaction within the x-y plane only).

C. Fermi surface

The Fermi surfaces of YB_4, shown in Fig. 6, will be representative of those of the trivalent RB_4 compounds although small differences may occur due to element-specific chemistry of trivalent rare earths and due to the lanthanide contraction. The large gap along the R-A-R edges precludes any Fermi surface on or near most of the $k_z=\frac{\pi}{c}$ face. The Fermi surfaces can be pictured as follows. Square hole pyramids with only slightly rounded vertices lie midway along the Γ-Z line, and similar nested electron pyramids lie along the M-A line near the M point. A pointed ellipsoid (football) oriented along k_z sits at the Z point. Surrounding Γ is a lens-type electron surface joined to pointed ellipsoids along the (110) directions. Finally, there are two "tortoise shell" shaped hole surfaces within the zone, located along the Γ-Z lines.

These surfaces, and the small variation through the lanthanide series, are surely relevant to the varying magnetic behavior observed in RB_4 compounds. There are nesting possibilities between the bases of the square pyramids, for example, which will appear as RKKY coupling as the associated nesting vectors. The ellipsoidal attachments on the zone-centered lens surface may provide some weak nesting.

V. LANTHANIDE SERIES

Any effective one-electron treatment of the electronic structure of $4f$ electron systems faces serious challenges. The root of the difficulty is that the ground state of an open $4f$ shell has intrinsic many-body character, being characterized by the spin S and angular momentum L of all of the $4f$ electrons, and the resulting total angular momentum J, following Hund's rules. Although it is possible to delve into the extent to which the LDA+U method can reproduce the z components of such configurations,[63] that is not the intention here. LDA+U reliably gets the high spin aspect, which contains much of the physics that determines relative $4f$ level positions and hence trends across the series. There is recent evidence from calculations on rare-earth nitrides[64] that, if spin-orbit coupling is neglected and the symmetry is lowered appropriately, the high orbital moment (Hund's second rule) can usually be reproduced. The exceptions are the usual difficult (and interesting) cases of Eu and Yb.

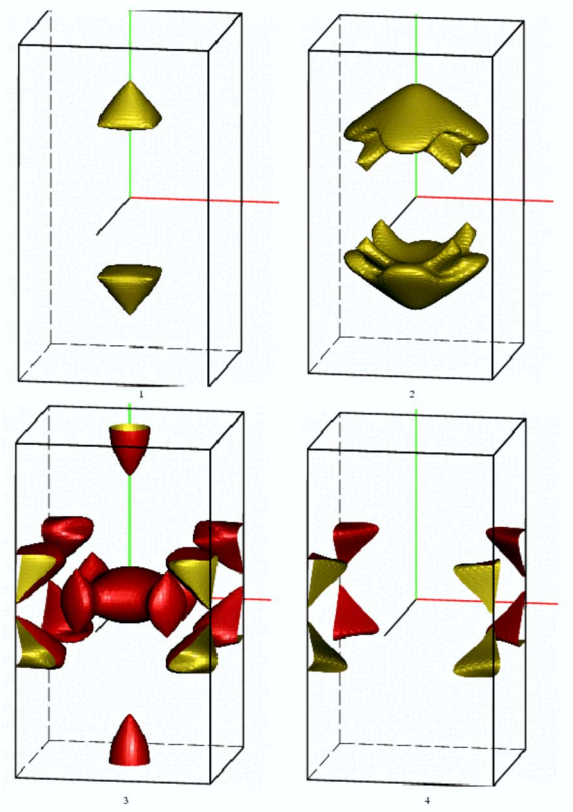

FIG. 6. (Color online) Fermi surfaces of YB_4. Light (yellow) surfaces enclose holes, and dark (red) surfaces enclose electrons. The full tetragonal Brillouin zone is pictured, the Γ point being in the center of each figure, the R point is the midpoint along the horizontal edges, and the A point lies at the corner (see Sec. III for specification of high symmetry points). The wide gap throughout the top and bottom edges of the zone accounts for the lack of Fermi surfaces except for the one "football" centered at the Z point at the center of the upper and lower faces (lower left panel).

Hund's rule ground state of the ion often breaks the local symmetry of the site, and if one is exploring that aspect the site symmetry should be allowed to be lower than the crystalline symmetry. As stated, we are not interested here in those details. In the calculations reported here, the crystal symmetry is retained. The site symmetry of the lanthanide ion is already low (mm), reflected in its 14-fold coordination with B atoms. In addition, spin-orbit coupling has not been included.

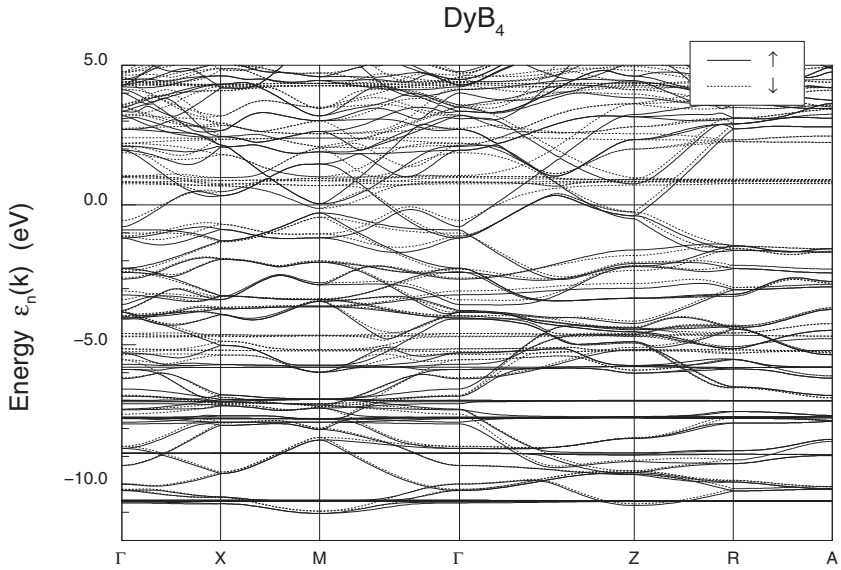

FIG. 7. The full valence band structure of DyB_4, and up to 5 eV in the conduction bands. This plot is for ferromagnetic alignment of the spin moments, with the solid bands being majority and the lighter, dashed lines showing the minority bands. The flatbands in the −4.5 to −11 eV are $4f$ eigenvalues as described by the LDA+U method.

A. Band structure

Most of the RB_4 lanthanide tetraborides follow the usual trivalent nature of these ions, and the itinerant parts of their band structures are very similar to those of YB_4 and LaB_4. The exceptions are R=Eu and Yb, which tend to be divalent to achieve a half-filled or filled shell, respectively.

By way of illustration of the complexity of the full RB_4 bands, the full band structure of DyB_4 is presented in Fig. 7 for ferromagnetic ordering. The $4f$ bands themselves can be identified by their flat (weakly hybridizing) nature. An enlarged picture of the bands within 1 eV of E_F is given in Fig. 8. The splitting of the majority and minority itinerant bands provides a direct measure of the Kondo coupling of the $4f$ moment to the band states. Note that the sign of this splitting can vary from band to band.

Figure 8 suggests that the Fermi surfaces will be different in the magnetic tetraborides (compared to YB_4) in specific ways. For Dy, the Γ-centered surface splits almost imperceptibly. The surfaces that cross the Γ-Z line also are relatively unaffected by exchange splitting. At the M point, however, a new surface appears due to the magnetism: an electron surface of minority spin. For this band, the polarization is opposite to the direction of the Dy spins. This figure is specifically for ferromagnetic alignment, while DyB_4 actually orders antiferromagnetically (see Sec. I).

B. Position of 4*f* levels

The mean position of $4f$ levels is displayed in Fig. 9, separated into occupied and unoccupied, and majority and minority, and trends are more meaningful than absolute energies. Simple ferromagnetic alignment is used here, in order to follow the chemical trends in the simplest manner. For the occupied majority states, the $4f$ level drops rapidly from Pr (−3 eV) to Sm (−7 eV), then becomes almost flat for Gd-Tm (around −8 eV). For the unoccupied minority states, the mean $4f$ level drops almost linearly from Pr (+5 eV) to Er

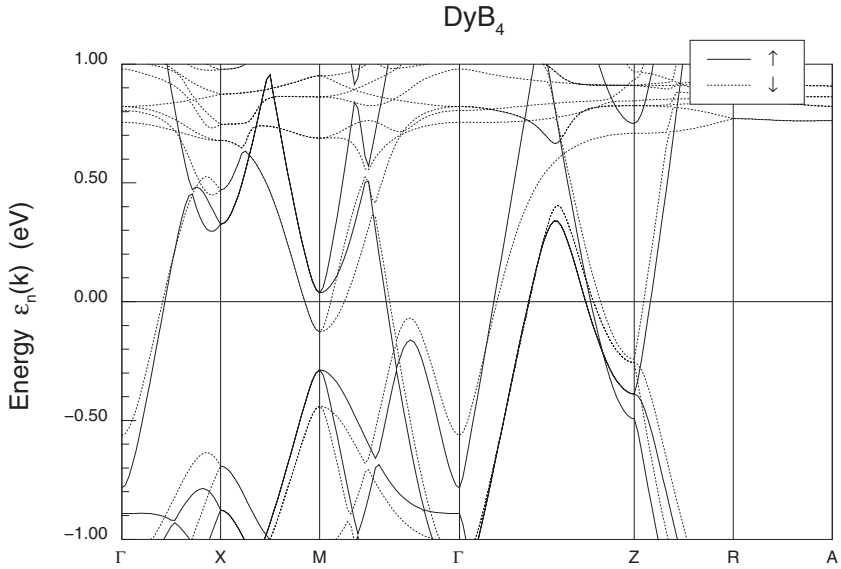

FIG. 8. Band structure of DyB_4 on a fine scale around the Fermi energy, see Fig. 7. The exchange splitting (between solid and dashed bands) gives a direct measure of the coupling between the polarized Dy ion and the itinerant bands (see text).

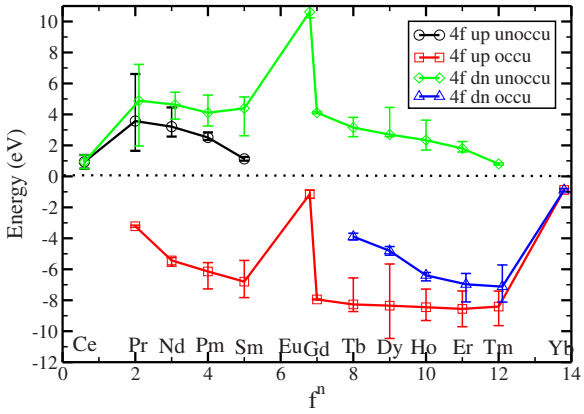

FIG. 9. (Color online) Calculated mean $4f$ eigenvalue position (symbols connected by lines) with respect to E_F, and the spread in eigenvalues, of RB_4 compounds. The smooth behavior from Pr to Tm (except for Eu) reflects the common trivalent state of these ions. Eu and Yb are calculated to be divalent and deviate strongly from the trivalent trend. Ce has a higher valence than 3, accounting for its deviation from the trivalent trend.

(+2 eV), and for Tm the $4f$ level is very close to E_F. The unoccupied majority levels, which become occupied minority levels beyond the middle of the series, drop more steeply, with slope almost −1 eV per unit increase in nuclear charge.

There are the usual exceptions to these overall trends. Ce is very different, indicating that it is very atypical (the calculational result is tetravalent and nonmagnetic). Both Eu and Yb are divalent in the calculation; an "extra" $4f$ state is occupied so their mean $4f$ level position is 6 eV (8 eV for Yb) higher than the trivalent line.

The spread in $4f$ eigenvalues is also displayed in Fig. 9. This spread is sensitive to the specific configuration that is obtained, and also has no direct relation to spectroscopic data, although it does reflect some of the internal potential shifts occurring in the LDA+U method. The distinctive features are the unusually large spread for the occupied majority levels in Dy (two electrons past half-filled shell), and for the unoccupied minority (and also unoccupied majority) levels in Pr (two electrons above the empty shell).

VI. SUMMARY

In this paper we have provided an analysis of the electronic structure of trivalent tetraborides, using YB_4 as the reference compound, and compared this with a divalent member CaB_4. In agreement with earlier observations on the likely bonding orbitals in the B atoms, it is found that bonding states are (nearly) filled and antibonding states are empty. The states at the Fermi level in the trivalent compounds are a combination of the (dimer) B2 p_z nonbonding orbitals whose bands pass through the bonding-antibonding gap, and the cation d orbitals. Since the extra electron in the trivalent compounds does not go into an antibonding state, there is no significant destabilization of the crystal structure.

The trends in the energy positions of the $4f$ states in the rare-earth tetraborides have been found to be consistent with expectations based on other rare-earth systems, as is the fact that Eu and Yb tend to be divalent rather than trivalent. Investigations of the magnetic behavior of rare-earth tetraborides will require individual study. Nearest neighbor magnetic interactions may involve a combination of $4f$-$4d$-$2p_z$-$4d$-$4f$ interactions, and longer range RKKY interactions that may bring in the Fermi surface geometry. Another possible coupling path is the direct $4f$-$2p_z$-$4f$ path. The coupling is likely to be even more complicated than in the rocksalt EuO and Eu chalcogenides, where competition between direct and indirect magnetic coupling paths has received recent attention.[65] The tetraboride structure is fascinating in several respects. A relevant one, if coupling does proceed directly via $4f$-$2p_z$-$4f$, is that the (dimer) B2 atom coordinates with *three* neighboring rare-earth ions, which will introduce frustration when the interaction has antiferromagnetic sign.

ACKNOWLEDGMENTS

We have benefited from discussion of the calculations with D. Kasinathan, K. Koepernik, and M. Richter, and from communication about data on DyB_4 with E. Choi. Support from the Alexander von Humboldt Foundation, and the hospitality of IFW Dresden, during the early part of this work is gratefully acknowledged. This work was supported by National Science Foundation Grant No. DMR-0421810.

[1] H. Nagamatsu, N. Hakagawa, T. Muranaka, Y. Zenitani, and J. Akimitsu, Nature (London) **410**, 63 (2001).
[2] J. M. An and W. E. Pickett, Phys. Rev. Lett. **86**, 4366 (2001).
[3] W. N. Lipscomb, J. Chem. Phys. **33**, 275 (1960).
[4] W. N. Lipscomb, J. Less-Common Met. **82**, 1 (1981).
[5] Y. Imai, M. Mukaida, M. Ueda, and A. Watanabe, Intermetallics **9**, 721 (2001).
[6] M. Takeda, T. Fukuda, F. Domingo, and T. Miura, J. Solid State Chem. **177**, 471 (2004).
[7] C.-H. Chen, T. Aizawa, N. Iyi, A. Sato, and S. Otani, J. Alloys Compd. **366**, L6 (2004).
[8] L. W. Rupp, Jr. and P. H. Schmidt, J. Phys. Chem. Solids **30**, 1059 (1969).
[9] S. Muranaka and S. Kawai, J. Cryst. Growth **26**, 165 (1974).
[10] J. L. Gavilano, B. Ambrosini, H. R. Ott, D. P. Young, and Z. Fisk, Physica B **281&282**, 428 (2000).
[11] J. L. Gavilano, B. Ambrosini, H. R. Ott, D. P. Young, and Z. Fisk, Physica B **284-288**, 1359 (2000).
[12] K. Schmitt, C. Stückl, H. Ripplinger, and B. Albert, Solid State Sci. **3**, 321 (2001).
[13] S. Otani, T. Aizawa, and Y. Yajima, J. Cryst. Growth **234**, 431 (2002).
[14] C.-H. Chen, Y. Xuan, and S. Otani, J. Alloys Compd. **350**, L4 (2003).

[15] P. Teredesai, D. V. S. Muthu, N. Chandrabhas, S. Meenakshi, V. Vijayakumar, P. Modak, R. S. Rao, B. K. Godwal, S. K. Sikka, and A. K. Sood, Solid State Commun. **129**, 91 (2004).
[16] S.-K. Mo, G.-H. Gweon, J. D. Denlinger, H.-D. Kim, J. W. Allen, C. G. Olson, H. Höchst, J. L. Sarrao, and Z. Fisk, Physica B **312-313**, 668 (2002).
[17] P. G. Perkins and A. V. J. Sweeney, J. Less-Common Met. **47**, 165 (1976).
[18] A. Ammar, M. Ménétrier, A. Villesuzanne, S. Matar, B. Chevalier, J. Etourneau, G. Villeneuve, J. Rodgiruez-Carvajal, H.-J. Koo, A. I. Smirnov, and M.-H. Whangbo, Inorg. Chem. **43**, 4974 (2004).
[19] Z. Fisk and M. B. Maple, Solid State Commun. **39**, 1189 (1981).
[20] J. Etourneau, J. Less-Common Met. **110**, 267 (1985).
[21] J. Etourneau, J. P. Mercurio, A. Berrada, and P. Hagenmuller, J. Less-Common Met. **67**, 531 (1979).
[22] Z. Fisk, A. S. Cooper, P. H. Schmidt, and R. N. Castellano, Mater. Res. Bull. **7**, 285 (1972).
[23] B. Jäger, S. Paluch, W. Wolf, P. Herzig, O. J. Zogal, N. Shitsevalova, and Y. Paderno, J. Alloys Compd. **383**, 232 (2004).
[24] S. Otani, Y. Xuan, Y. Yajima, and T. Mori, J. Alloys Compd. **361**, L1 (2003).
[25] S. Otani, M. M. Korsukova, T. Mitsuhashi, and N. Kieda, J. Cryst. Growth **217**, 378 (2000).
[26] T. Tanaka and Yoshio Ishizawa, J. Phys. C **18**, 4933 (1985).
[27] J. Günster, T. Tanaka, and R. Souda, Phys. Rev. B **56**, 15962 (1997).
[28] K. Kato, I. Kawada, C. Oshima, and S. Kawai, Acta Crystallogr., Sect. B: Struct. Crystallogr. Cryst. Chem. **B30**, 2933 (1974).
[29] S. V. Meschel and O. J. Kleppa, J. Alloys Compd. **226**, 243 (1995).
[30] A. Zalkin and D. H. Templeton, Acta Crystallogr. **6**, 269 (1953).
[31] A. Zalkin and D. H. Templeton, J. Chem. Phys. **18**, 391 (1950).
[32] P. Salamakha, A. P. Goncalves, O. Sologub, and M. Almeida, J. Alloys Compd. **316**, L4 (2001).
[33] B. J. Mean, K. H. Kang, J. H. Kim, I. N. Hyun, M. Lee, and B. K. Cho, Physica B **378-380**, 598 (2006).
[34] S. Ji, C. Song, J. Koo, K.-B. Lee, Y. J. Park, J. Y. Kim, J.-H. Park, H. J. Shin, J. S. Rhyee, B. H. Oh, and B. K. Cho, Phys. Rev. Lett. **91**, 257205 (2003).
[35] M. T. Garland, J. P. Wiff, J. Bauer, R. Guerin, and J.-Y. Saillard, Solid State Sci. **5**, 705 (2003).
[36] K. H. J. Buschow and J. H. N. Creighton, J. Chem. Phys. **57**, 3910 (1972).
[37] S. W. Lovesey, J. Fernandez Rodrğuez, J. A. Blanco, and P. J. Brown, Phys. Rev. B **70**, 172414 (2004).
[38] J. A. Blanco, P. J. Brown, A. Stunault, K. Katsumata, F. Iga, and S. Michimura, Phys. Rev. B **73**, 212411 (2006).
[39] B. J. Mean, K. H. Kang, J. H. Kim, I. N. Hyun, M. Lee, and B. K. Cho, Physica B **378-380**, 600 (2006).
[40] J. C. Gianduzzo, R. Georges, B. Chevalier, J. Etourneau, P. Hagenmuller, G. Will, and W. Schäfer, J. Less-Common Met. **82**, 29 (1981).
[41] F. Elf, W. Schäfer, and G. Will, Solid State Commun. **40**, 579 (1981).
[42] Z. Heiba, W. Schäfer, E. Jansen, and G. Will, J. Phys. Chem. Solids **47**, 651 (1986).
[43] G. Will, W. Schäfer, F. Pfeiffer, and F. Elf, J. Less-Common Met. **82**, 349 (1981).
[44] G. Will, Z. Heiba, W. Schäfer, and E. Jansen, Ann. Isr. Phys. Soc. **140**, 130 (1986).
[45] D. Okuyama, T. Matsumura, H. Nakao, and Y. Murakami, J. Phys. Soc. Jpn. **74**, 2434 (2005).
[46] R. Watanuki, H. Mitamura, T. Sakakibara, G. Sato, and K. Suzuki, Physica B **378-380**, 594 (2006).
[47] T. Matsumura, D. Okuyama, H. Nakao, and Y. Murakami, Photon Factory Activity Report 2004 No. 24 Part B, 2005 (unpublished).
[48] E. M. Dudnik, Y. A. Kochierzhinsky, Y. B. Paderno, N. Y. Shitsevalova, E. A. Shishkin, and I. E. Kir'yakova, J. Less-Common Met. **67**, 281 (1979).
[49] W. Schäfer, G. Will, and K. H. J. Buschow, J. Magn. Magn. Mater. **3**, 61 (1976).
[50] R. Watanuki, G. Sato, K. Suzuki, M. Ishihara, T. Yanagisawa, Y. Nemoto, and T. Goto, J. Phys. Soc. Jpn. **74**, 2169 (2005).
[51] G. Will and W. Schäfer, J. Less-Common Met. **67**, 31 (1979).
[52] L. I. Derkachenko, V. N. Gurin, and M. M. Korsukova, J. Solid State Chem. **133**, 296 (1997).
[53] R. Schmitt, B. Blaschkowski, K. Eichele, and H. J. Meyer, Inorg. Chem. **45**, 3067 (2006).
[54] D. R. Noakes, G. K. Shenoy, D. Niarchos, A. M. Umarji, and A. T. Aldred, Phys. Rev. B **27**, 4317 (1983).
[55] P. C. Canfield, S. L. Bud'ko, B. K. Cho, W. P. Beyermann, and A. Yatskar, J. Alloys Compd. **250**, 596 (1997).
[56] M. A. Ruderman and C. Kittel, Phys. Rev. **96**, 99 (1954); T. Kasuya, Prog. Theor. Phys. **16**, 45 (1956); K. Yosida, Phys. Rev. **106**, 893 (1957).
[57] K. Koepernik and H. Eschrig, Phys. Rev. B **59**, 1743 (1999).
[58] J. P. Perdew and Y. Wang, Phys. Rev. B **45**, 13244 (1992).
[59] D. Okuyama, T. Matsumura, H. Nakao, and Y. Murakami, J. Phys. Soc. Jpn. **75**, 198 (2006).
[60] A. Kokalj, Comput. Mater. Sci. **28**, 155 (2003). The code is available from http://www.xcrysden.org/
[61] T. Lundström, Pure Appl. Chem. **57**, 1383 (1985).
[62] A. Vegas, L. A. Martinez-Cruz, A. Ramos-Gallardo, and A. Romero, Z. Kristallogr. **210**, 574 (1995).
[63] M. D. Johannes and W. E. Pickett, Phys. Rev. B **72**, 195116 (2005).
[64] P. Larson, W. R. L. Lambrecht, A. Chantis, and M. van Schilfgaarde, Phys. Rev. B **75**, 045114 (2007).
[65] J. Kuneš and W. E. Pickett, J. Phys. Soc. Jpn. **74**, 1408 (2005).